JPE 17-2-25

https://doi.org/10.6113/JPE.2017.17.2.570
ISSN(Print): 1598-2092 / ISSN(Online): 2093-4718

Secondary Side Output Voltage Stabilization of an IPT System by Tuning/Detuning through a Serial Tuned DC Voltage-controlled Variable Capacitor

Jianlong Tian†, Aiguo Patrick Hu*, and Sing Kiong Nguang**

†,*Department of Electrical and Computer Engineering, The University of Auckland, Auckland, New Zealand

Abstract

This paper proposes a method to stabilize the output voltage of the secondary side of an Inductive Power Transfer (IPT) system through tuning/detuning via a serial tuned DC Voltage-controlled Variable Capacitor (DVVC). The equivalent capacitance of the DVVC changes with the conduction period of a diode in the DVVC controlled by DC voltage. The output voltage of an IPT system can be made constant when this DVVC is used as a variable resonant capacitor combined with a PI controller generating DC control voltage according to the fluctuations of the output voltage. Since a passive diode instead of an active switch is used in the DVVC, there are no active switch driving problems such as a separate voltage source or gate drivers, which makes the DVVC especially advantageous when used at the secondary side of an IPT system. Moreover, since the equivalent capacitance of the DVVC can be controlled smoothly with a DC voltage and the passive diode generates less EMI than active switches, the DVVC has the potential to be used at much higher frequencies than traditional switch mode capacitors.

Key words: Inductive power transfer, Output voltage stabilization, Pick-up circuit tuning, Wireless power transfer

I. INTRODUCTION

The output voltage of a wireless power transfer (WPT) system can be made constant by either primary or secondary side control [1], [2]. Since a separate communication channel is normally needed for primary side control [3]-[10], it is more straightforward to directly regulate the output voltage at the secondary side [11]-[18]. In [11]-[13], an active switch is used to short the secondary side circuit to regulate the power flow and to stabilize the output voltage. Such methods involve active switching, which usually happens when the current of the circuit is large, which generates large switching noise and power losses, and causes ripples at the output. An alternative method is to operate a power transistor in the linear region to form a variable resistor in series with a tuning capacitor [14]-[16]. This has the advantages of smooth power regulation and low EMI. However, the regulation of its equivalent capacitance relies solely on changing the resistance of the power transistor in its linear region. Therefore, this type of method is not suitable for a wide range of regulation due to the high power losses associated.

This paper proposes a method to directly stabilize the output voltage at the secondary side through a DC Voltage-controlled Variable Capacitor (DVVC), which combines the features of both linear and switching mode operation by controlling the conduction period of a diode (passive switch) through a transistor (works in the linear mode). The equivalent capacitance of the DVVC changes with variations of the conduction period of the diode. The on-off state transition of the diode happens naturally with voltage and current oscillations of the circuit when they drop to zero, which makes the switching condition of the DVVC much better than that of traditional switch mode capacitors. Another advantage of the DVVC is its simple structure. Because no active switches are used, so no gate drivers and a high, up to 20V, separate voltage source are needed, which makes the DVVC especially advantageous when used at the secondary side of an IPT system.

This paper is organized as follows. The basic operating principle of the DVVC is explained in section II. Section III presents the theoretical modelling and analysis. Simulation

Manuscript received Apr. 2, 2016; accepted Dec. 21, 2016
Recommended for publication by Associate Editor Jee-Hoon Jung.
†Corresponding Author: jtia983@aucklanduni.ac.nz
Tel: +64-9-022 068 6690, The University of Auckland
*Department of Electrical and Computer Engineering, The University of Auckland, New Zealand

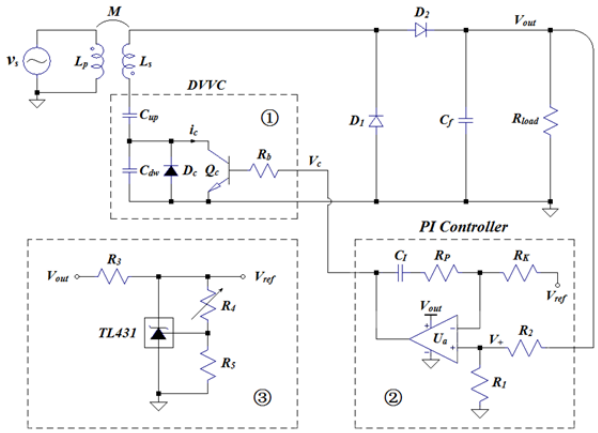

Fig. 1. The proposed pick-up output voltage stabilization method through the *DVVC* and a *PI controller*.

results are provided in section IV. Section V presents some practical experimental results. Finally conclusions are drawn in section VI.

II. The Proposed Method and Basic Operating Principle

Fig. 1 shows the proposed DC Voltage-controlled Variable Capacitor (*DVVC*) applied in the secondary side of an IPT system combined with a PI Controller.

The *DVVC* includes C_{up}, C_{dw}, D_c, Q_c and R_b as shown in the dashed circuit block numbered ① in Fig. 1. The PI Controller is shown in the dashed circuit block numbered ② in Fig. 1. It includes C_I, R_P, R_K, R_1, R_2 and U_a. The dashed circuit block numbered ③ in Fig. 1 shows the circuitry (centered on an adjustable precision shunt regulator TL431) to generate the reference voltage V_{ref} for the PI Controller. To concentrate on studying the performance and characteristics of the *DVVC* at the secondary side, the primary side simply uses a power amplifier v_s to generate a sinusoidal current at a fixed frequency to drive the primary coil L_p. The secondary side of the system is a serial tuned half-bridge rectification pick-up where the common fixed value tuning capacitor is replaced by the *DVVC*. The capacitance of this *DVVC* is C_{up} when the diode D_c is on, and C_{up} and C_{dw} in series when the diode D_c is off, because when D_c is on, the capacitor C_{dw} and transistor Q_c are short-circuited by the conducting diode, and when D_c is off, it can be regarded as open so that C_{up} and C_{dw} become in series. Since the capacitance of C_{up} is larger than the capacitance of C_{up} and C_{dw} in series, the longer the diode conducts, the larger the average equivalent capacitance of the *DVVC* becomes, which changes between C_{up} and the value of C_{up} and C_{dw} in series according to the conduction period T_{con} of the diode D_c.

The conduction period T_{con} of the diode D_c can be controlled by the voltage V_c through its influence on the base and collector currents i_b and i_c of the transistor Q_c. The collector current i_c of Q_c in turn affects the voltage across the diode D_c. The higher V_c is, the larger i_b and i_c become. The larger i_c is, the lower the voltage across the diode D_c becomes because i_c plays a role to pull the voltage on the cathode of the diode down to the ground. A lower voltage across the diode D_c leads to a longer conduction period T_{con} of the diode and a larger equivalent capacitance of the *DVVC*. Therefore, the voltage V_c controls the equivalent capacitance of the *DVVC* by affecting the conduction period T_{con} of the diode through its influence on i_b, i_c and the voltage across the diode D_c. The higher V_c is, the longer the diode conducts and the larger the average equivalent capacitance of the *DVVC* becomes.

In Fig. 1, the output voltage of the secondary side of the IPT system changes with variations of the tuning capacitance, and there is a value for the tuning capacitance (C_{vmax}) at which the output voltage reaches its maximum. The relationship between the tuning capacitance and the output voltage is monotonic if the tuning capacitance changes between 0 and C_{vmax} or between C_{vmax} and ∞. Since the application of a PI controller to stabilize the output voltage by adjusting the equivalent capacitance of the *DVVC* requires that there is a monotonic relationship between the equivalent capacitance of the *DVVC* and the output voltage, the equivalent capacitance of the *DVVC* should be designed to vary within a range that is either higher or lower than C_{vmax}. In this paper, the tuning capacitance is designed to change between C_{vmax} and ∞ by making the smallest value of the equivalent capacitance of the *DVVC* C_{min}, i.e. C_{up} and C_{dw} in series, as expressed by (1), is larger than C_{vmax} so that the pickup circuit is always over tuned when the control voltage V_c is not zero.

$$C_{min} = \frac{C_{up}C_{dw}}{C_{up} + C_{dw}} \tag{1}$$

The value of the tuned capacitance C_{vmax} at which the output voltage reaches its maximum is very complex for the half-bridge regulation pick-up circuit. It cannot be simply determined by the value of the inductor and capacitor of the resonant tank. Therefore, it is usually determined through experimentation.

Since the higher V_c is, the larger the equivalent capacitance of the *DVVC* becomes, when $C_{min} > C_{vmax}$, a higher V_c leads to a lower output voltage, which can be seen in the simulation and experimental results as shown in Fig. 8 (section IV) and Fig. 12 (section V), respectively.

The function of the PI Controller is to automatically generate the controlling voltage V_c according to the fluctuation of the output voltage V_{out} to make V_{out} constant. As can be seen in Fig. 1, the feedback signal from the output voltage V_{out} is input into the "non-inverting" terminal of the op-amp U_a of the PI Controller. As a result, the higher the output voltage V_{out} is, the higher the controlling voltage V_c (the output of the PI Controller) becomes. This makes the equivalent capacitance of the *DVVC* larger. Therefore, it further deviates from the tuned capacitance C_{vmax} so that the output voltage V_{out} becomes

smaller. When the output voltage V_{out} gets lower than the set value, the process reverses. In short, it is a negative feedback loop for controlling the output voltage V_{out} by the tuning/detuning effect of the *DVVC*.

Fig. 1 shows that the output voltage V_{out} can be used directly as the source of the op-amp U_a of the PI Controller, which simplifies the whole circuitry and is especially advantageous at the secondary side of an IPT system. The two resistors R1 and R2 are voltage dividers of the output voltage V_{out} for generating the feedback signal V_+ for the op-amp U_a. Their values can be designed to make V_+ roughly equal to the reference voltage V_{ref} according to the set value of the output voltage V_{out}. The reference voltage V_{ref} is generated by an adjustable precision shunt regulator TL431 in this paper. The output voltage V_{out} can be adjusted finely by tuning the output voltage of the TL431 through the variable resistor R4 after the values of R1 and R2 are fixed.

III. Theoretical Modeling and Analysis

As previously explained, the reason the voltage V_c can control the average equivalent capacitance of the *DVVC* is that V_c influences the conduction period T_{con} of the diode D_c. Therefore, the relationship between T_{con} and V_c is the basis of the theoretical analysis. To find the relationship between T_{con} and V_c, the circuit is modelled like those shown in Fig. 2 (a) and (b) representing the two situations when the diode is on and off, respectively, where v_{ss} represents the voltage induced in the secondary side coil L_s. The original rectification circuit, the filter capacitor C_f, and the DC load R_{load} are simplified together as an AC load R_{ac}.

Fig. 3 shows typical waveforms of v_{ss}, i_s, v_{Cdw} and i_{Dc} (the current flowing through the diode D_c), from which it can be seen that the current i_s is zero at the moments "t_{off}" when the diode stops conducting, and that the voltage v_{Cdw} is zero at both of the moments "t_{on}" and "t_{off}" when the diode D_c starts and stops conducting. This means that zero voltage switching (ZVS) is achieved when the diode turns on and both ZVS and zero current switching (ZCS) are achieved when the diode turns off.

To determine the relationship between T_{con} and V_c, two exact moments, i.e. the moment the diode starts to conduct "t_{on}" and the moment the diode stops conducting "t_{off}", need to be determined first. Then, T_{con} can be calculated with (2):

$$T_{con} = t_{off} - t_{on} \tag{2}$$

The moment "t_{off}" can be found with the circuit when the diode is on, as shown in Fig. 2 (a), where C_{dw}, D_c and Q_c are removed because an ideal conducting diode is equivalent to a short-circuit. The moment the diode stops conducting "t_{off}" is regarded as when the current flowing through the diode at the moment-i_s drops to zero. Suppose that the voltage source v_{ss} is expressed by (3) (refer to Fig. 3 (a)).

$$v_{ss} = V_m cos\omega t \tag{3}$$

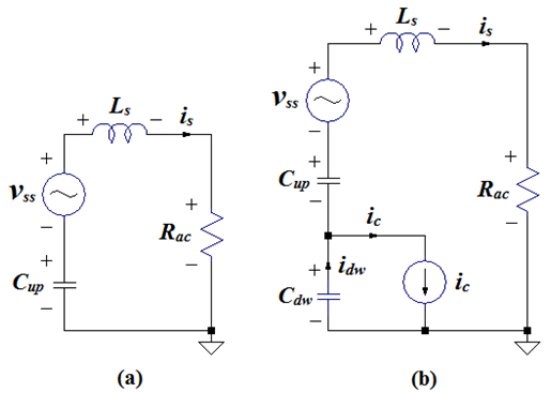

Fig. 2. The simplified equivalent circuit when the diode is on (a) and off (b), respectively.

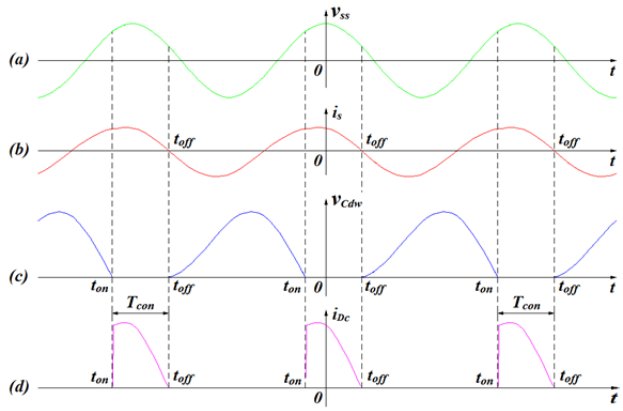

Fig. 3. The typical wave forms of v_{ss}, i_s, v_{Cdw} and i_{Dc}.

The differential equation governing i_s is:

$$L_s C_{up} \frac{d^2 i_s}{dt^2} + R_{ac} C_{up} \frac{di_s}{dt} + i_s = -C_{up} V_m \omega sin\omega t \tag{4}$$

When $R_{ac} > 2\sqrt{\frac{L_s}{C_{up}}}$, the full solution of (4) can be expressed by (5) (refer to Fig. 3 (b)).

$$i_s = A_1 e^{r_1 t} + A_2 e^{r_2 t} + A cos\omega t + B sin\omega t \tag{5}$$

where:

$$r_{1,2} = -\frac{R_{ac}}{2L_s} \pm \sqrt{\left(\frac{R_{ac}}{2L_s}\right)^2 - \frac{1}{L_s C_{up}}}$$

$$A = \frac{V_m R_{ac} {C_{up}}^2 \omega^2}{\left(1 - L_s C_{up}\omega^2\right)^2 + \left(R_{ac} C_{up}\omega\right)^2}$$

$$B = \frac{V_m C_{up}\omega\left(L_s C_{up}\omega^2 - 1\right)}{\left(1 - L_s C_{up}\omega^2\right)^2 + \left(R_{ac} C_{up}\omega\right)^2}$$

and *A1* and *A2* are integral constants which need to be determined by the initial conditions.

It can be seen from the typical waveforms shown in Fig. 3 (b) that i_s is zero at the moment "t_{off}", which can be expressed by (6), which governs the moment "t_{off}" when the diode turns off:

$$A_1 e^{r_1 t_{off}} + A_2 e^{r_2 t_{off}} + A cos\omega t_{off} + B sin\omega t_{off} = 0 \tag{6}$$

The moment "t_{on}" can be found with the circuit when the diode is off, as shown in Fig. 2 (b), where the diode D_c is removed because it amounts to an open-circuit when it is off,

and the transistor Q_c is modelled as a constant current source i_c controlled by the voltage V_c with the relationship:

$$i_c = \beta \cdot i_b = \beta \cdot \frac{V_c}{R_b} \tag{7}$$

The moment the diode starts to conduct "t_{on}" is regarded as when the voltage across the diode v_{Cdw} drops to zero. To determine v_{Cdw}, i_{dw} needs to be found first, which is governed by (8):

$$\frac{d^2 i_{dw}}{dt^2} + \frac{R_{ac}}{L_s} \cdot \frac{di_{dw}}{dt} + \frac{1}{L_s C_{updw}} \cdot i_{dw} = \frac{i_c}{L_s C_{up}} - \frac{V_m \omega}{L_s} sin\omega t \tag{8}$$

When $R_{ac} > 2\sqrt{\frac{L_s}{C_{updw}}}$, the full solution of (8) is:

$$i_{dw} = B_1 e^{r_1' t} + B_2 e^{r_2' t} + A' cos\omega t + B' sin\omega t + \frac{\beta}{R_b}\left(\frac{C_{up}}{C_{up} + C_{dw}}\right) \cdot V_c \tag{9}$$

where:

$$C_{updw} = \frac{C_{up} C_{dw}}{C_{up} + C_{dw}}$$

$$r_{1,2}' = -\frac{R_{ac}}{2L_s} \pm \sqrt{\left(\frac{R_{ac}}{2L_s}\right)^2 - \frac{1}{L_s C_{updw}}}$$

$$A' = \frac{V_m R_{ac} {C_{updw}}^2 \omega^2}{\left(1 - L_s C_{updw} \omega^2\right)^2 + \left(R_{ac} C_{updw} \omega\right)^2}$$

$$B' = \frac{V_m C_{updw} \omega \left(L_s C_{updw} \omega^2 - 1\right)}{\left(1 - L_s C_{updw} \omega^2\right)^2 + \left(R_{ac} C_{updw} \omega\right)^2}$$

and *B1* and *B2* are integral constants which need to be determined by the initial conditions.

The relationship between "i_{dw}" and "v_{Cdw}" is governed by (10):

$$v_{Cdw} = -\frac{1}{C_{dw}} \int i_{dw} + K \tag{10}$$

Substituting (9) into (10) and calculating the indefinite integral of *idw* leads to (11) where K is the integral constant which needs to be determined by the initial conditions. A waveform of "v_{Cdw}" is shown in Fig. 3 (c), from which it can be seen that v_{Cdw} is zero at the moment "*ton*" when the diode starts to conduct, which is expressed by (12), which governs the moment "t_{on}" when the diode starts to conduct.

$$v_{Cdw} = -\frac{1}{C_{dw}}\left(\frac{B_1}{r_1'} e^{r_1' t} + \frac{B_2}{r_2'} e^{r_2' t} + \frac{A'}{\omega} sin\omega t - \frac{B'}{\omega} cos\omega t + \frac{C_{up} \beta V_c}{R_b\left(C_{up} + C_{dw}\right)} \cdot t\right) + K \tag{11}$$

$$-\frac{1}{C_{dw}}\left(\frac{B_1}{r_1'} e^{r_1' t_{on}} + \frac{B_2}{r_2'} e^{r_2' t_{on}} + \frac{A'}{\omega} sin\omega t_{on} - \frac{B'}{\omega} cos\omega t_{on} + \frac{C_{up} \beta V_c}{R_b\left(C_{up} + C_{dw}\right)} \cdot t_{on}\right) + K = 0 \tag{12}$$

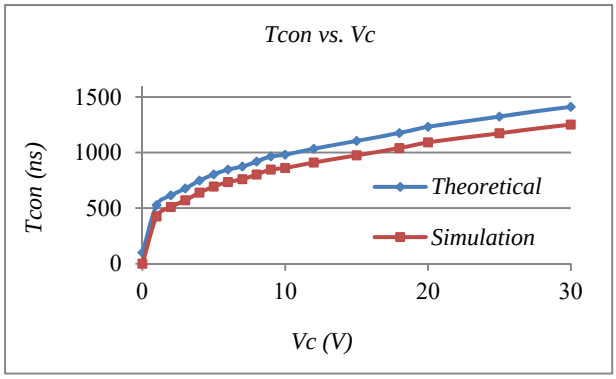

Fig. 4. The theoretical and simulation relationship between T_{con} and the control voltage V_c with the same AC load of 100Ω.

It can be seen from (6) and (12) that there are no analytical solutions for "t_{on}" and "t_{off}". As a result, numerical solutions (for example using Matlab) are needed. With both "t_{on}" and "t_{off}" available, T_{con} can be calculated with (2).

The theoretical and simulated relationship between T_{con} and the control voltage V_c are shown in Fig. 4, from which it can be seen that they agree with each other quite well. There are small errors that are caused by multi-factors such as the idealization of the components of the circuit in the theoretical analysis, especially the current gain of the transistor. The differences in the actual gain and other parameters of the transistor between the theoretical assumptions and simulation can result in errors. In addition, another cause of errors between the theoretical and simulation results is related to the amplitude of v_{ss}, which is assumed to be constant in the theoretical analysis. However, it actually varies in component level simulations and practical circuit experimentation because of the change of the equivalent capacitance of the *DVVC* with the control voltage V_c.

It should be noted that only the overdamping situation, when $R_{ac} > 2\sqrt{\frac{L_s}{C_{up}}}$ and $\mathrm{R_{ac}} > 2\sqrt{\frac{\mathrm{L_S}}{\mathrm{C_{updw}}}}$, is discussed in this paper, and that the same method can be used for analyzing under and critical damping conditions.

IV. Simulation Study

The components and parameters of the circuit used in the simulation are the same as those used in the practical experiments as shown in Table 1 of the next section. To reveal the principle that the higher the control voltage V_c is, the higher the collector current i_c becomes, and that the higher i_c is, the lower the voltage across the diode v_{Cdw} becomes and the longer the diode conducts; Fig. 5 shows the simulated waveforms of i_c, v_{Cdw} and i_{Dc} (the current flowing through the diode D_c) when the control voltage V_c is 5V (Fig. 5 (a), (b) and (c)) and 20V (Fig. 5 (d), (e) and (f)), respectively.

It can be seen from Fig. 5 that the amplitude of i_c when V_c

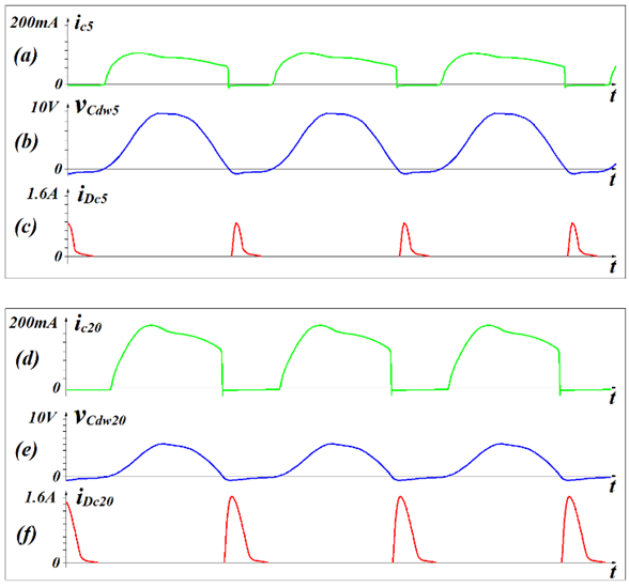

Fig. 5. Typical waveforms i_c, v_{Cdw} and i_{Dc} when the control voltage V_c is set at 5V and 20V, respectively.

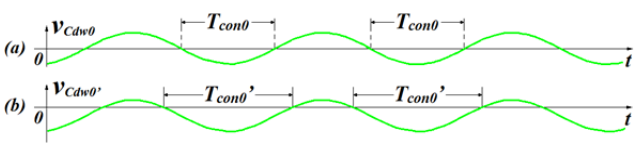

Fig. 6. Typical waveforms v_{Cdw} when the diode and transistor are removed from the circuit.

is 20V is higher than that when V_c is 5V, the amplitude of v_{Cdw} when V_c is 20V is lower than that when V_c is 5V, and the conduction period T_{con} when V_c is 20V is longer than that when V_c is 5V.

Fig. 6 (a) shows the voltage v_{Cdw} when the diode D_c, the transistor Q_c and the base resistor R_b are removed from the circuit and there are only the two capacitors C_{up} and C_{dw} left. Fig. 6 (b) shows the voltage v_{Cdw} when v_{Cdw0}, shown in Fig. 6 (a), is moved downwards along the Y-axis. It can be seen from Fig. 6 (a) and (b) that after it is moved downwards, or in other words, when the voltage is lowered, the length of the negative parts of the voltage (referring to Fig. 3 (c), the negative parts will be zero if a diode is present and the length of this part represents the conduction period T_{con} of the diode) along the X-axis becomes longer ($T_{con0}' > T_{con0}$). This shows why when the amplitude of the voltage across the diode D_c is lowered, its conduction period becomes longer. In summary, the control voltage V_c makes the conduction period of the diode D_c longer by making the voltage across the diode lower.

Since the conduction period T_{con} of the diode D_c plays a central role and is the fundamental reason why the control voltage V_c can change the equivalent capacitance of the *DVVC* and the output voltage, Fig. 7 shows the simulated relationship between T_{con} and V_c under different values of the base resistor R_b.

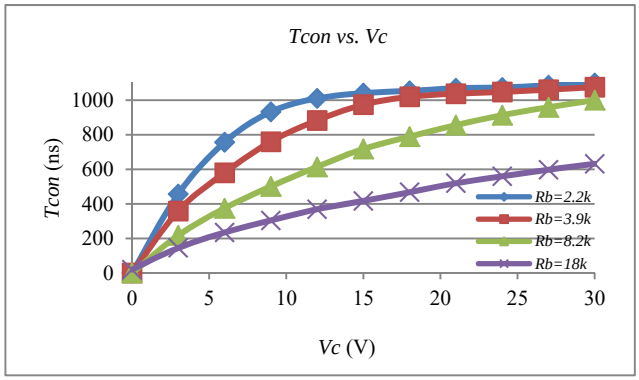

Fig. 7. The simulated relationships between T_{con} and V_c under different values of R_b.

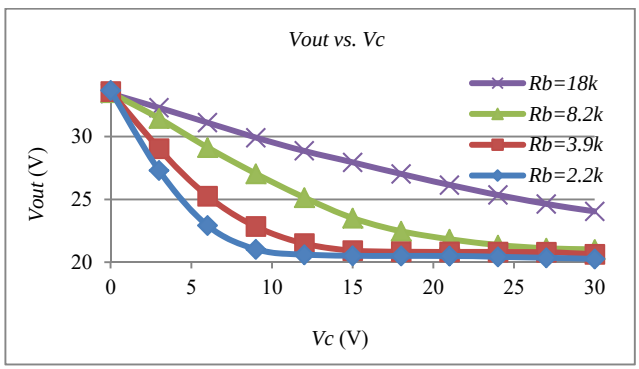

Fig. 8. The simulated relationship between V_{out} and V_c under different values of R_b.

It can be seen from Fig. 7 that T_{con} is proportionate to V_c, and that at the same value of V_c, the smaller R_b is, the larger the corresponding T_{con} becomes, which means the influence of V_c on the conduction period of the diode is stronger. This is because the smaller R_b is, the larger the base and collector current i_b and i_c of the transistor Q_c become. A higher i_c pulls the level of the voltage across the diode lower so that the diode conducts longer. Actually, both V_c and R_b influence the diode conduction period T_{con} through their impact on the base and collector currents i_b and i_c.

Fig. 8 shows the simulated relationships between the output voltage V_{out} and the control voltage V_c under different values of the base resistor R_b. It can be seen from this figure that a higher V_c leads to a lower V_{out}, which is in consistent with the analysis in section II and the simulation result shown in Fig. 5, from which it can be seen that a higher V_c leads to a longer T_{con}. As explained in section II, a longer T_{con} leads to a larger equivalent capacitance of the *DVVC* which makes the pick-up circuit detuned more seriously. As a result, the output voltage becomes lower.

Fig. 9 shows simulated waveforms of the output voltage V_{out} and the control voltage V_c when a simple PI controller is added to generate V_c according to the fluctuations of the output voltage V_{out} caused by variations of the load resistance, which are controlled to change periodically between 50Ω

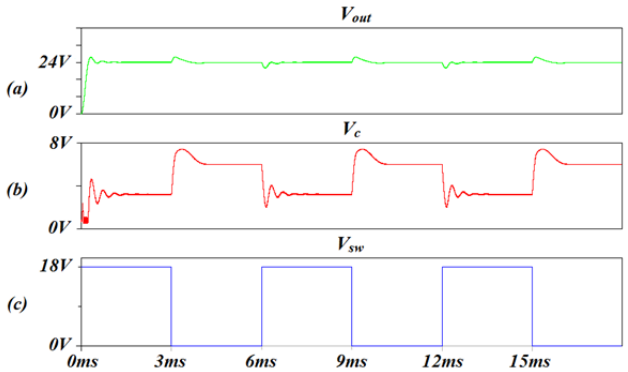

Fig. 9. The simulated waveforms of V_{out}, V_c and the switching signal V_{sw} with which the load resistance R_{load} is changed periodically between 50Ω and 100Ω.

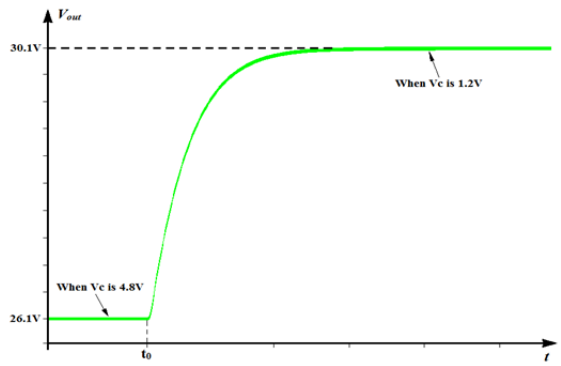

Fig. 10. The simulated open loop step response of the circuit as shown in Fig. 1.

and 100Ω with a switch. Fig. 9 (a), (b) and (c) show the output voltage V_{out}, control voltage V_c and switching signal V_{sw}, respectively. From these figures it can be seen that at the switching moments, the control voltage V_c responds immediately to keep the output voltage constant at the designed value of 24V. The output voltage V_{out} has only small fluctuations when the load resistance is changed suddenly.

The Ziegler-Nichols tuning method [19], [20] is used to determine the initial parameters for the PI controller. The step response of the system (V_c as the input changing from 4.8V to 1.2V, and V_{out} as the output) is obtained by a simulation, as shown in Fig. 10, and then the parameters of the PI controller are calculated as K_p=6.726 and T_i=6.46e-5 through empirical formulas [21], [22]. The transfer function of the PI controller of the Ziegler-Nichols method is in the form of:

$$H(s) = K_p(1 + \frac{1}{s \cdot T_i}) \tag{13}$$

The transfer function of the PI controller, in Fig. 1 of this paper, is in the form of:

$$H_1(s) = K_{p1}(1 + \frac{1}{s \cdot T_{i1}}) \tag{14}$$

where:

$$K_{p1} = \frac{R_1(R_p + R_k)}{(R_1 + R_2)R_k} \tag{15}$$

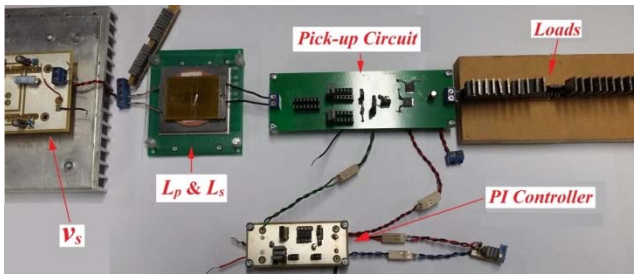

Fig. 11. The experimental setup.

TABLE I
Components AND Paramiters of the Circuit Used in the Simulation AND Experiments

Frequency of v_s (kHz)	L_p (uH)	L_s (uH)	C_{up} (nF)	C_{dw} (nF)	D_c, D_1, D_2
240	24	10	100	100	BYV26C
Amplitude of v_s (V)	k	Q_c	R_b (kΩ)	C_f (uF)	R_{load} (Ω)
15	0.66	KSE13003	18	10	100
C_I (nF)	R_P (kΩ)	R_K (kΩ)	Ua	R_1 (kΩ)	R_2 (kΩ)
0.33	200	3	LM358	20	180

$$T_{i1} = (R_p + R_k)C_I \tag{16}$$

Equating (13) and (14) gives:

$$K_{p1} = K_p \tag{17}$$

$$T_{i1} = T_i \tag{18}$$

Based on the Ziegler-Nichols method, the PI controller is fine-tuned for better performance. The practical values of K_{p1} and T_{i1} are chosen as 6.76 and 6.7e-5, respectively. The final practical circuit parameters of the PI controller in relation to (15) and (16) are shown in Table 1 of Section V.

V. Experimental Results

Fig. 11 shows the experimental setup including the power amplifier v_s, the primary and secondary side coils L_p & L_s, the pick-up circuit, the loads and the PI controller.

Table 1 show the components and parameters of the circuit used in the simulations and experiments.

An open-loop experiment with the control voltage V_c generated by a voltage source is carried out to determine the relationship between the output voltage V_{out} and V_c under different values of the base resistor R_b. The results are shown in Fig. 12. They agree quite well with the simulation results shown in Fig. 8 with errors of about ±4.6% to ±0.07% for different values of R_b and V_c.

It can be seen from Fig. 12 that the output voltage changes greatly (about 12 volts, roughly from 21V to 33V) with variations of the control voltage V_c. Another feature that can be seen from Fig. 12 is that the smaller R_b is, the sharper the output voltage changes with a change of the control voltage V_c. This is because the smaller R_b is, the more influence the control voltage V_c has on the collector current i_c, the voltage

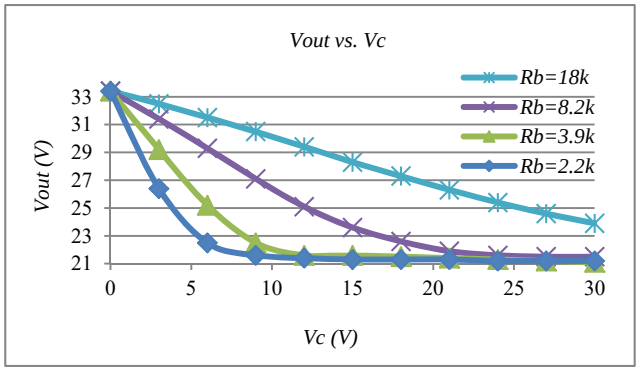

Fig. 12. Experimental relationships between V_{out} and V_c with R_b at different values.

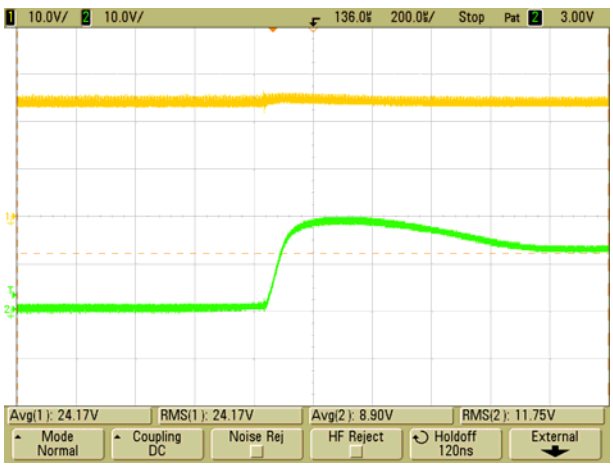

Fig. 13. The transient waveforms of V_{out} (top) and V_c (bottom) when the load changes suddenly from 50Ω to 100Ω.

across the diode D_c and the conduction period T_{con} of the diode. R_b should be designed to be small enough to make V_c have sufficient control over the output voltage so that the adjustable range of the output voltage is large enough. Within the adjustable range of the output voltage, a larger R_b makes the system more stable.

A separate experiment with the PI controller added is carried out to test the closed-loop performance of the proposed method. The output voltage V_{out} is designed to be 24V and it is directly used as the voltage source of the PI controller in the experiment. Fig. 13 shows transient experimental waveforms of the output voltage V_{out} (yellow near the top) and the control voltage V_c (green near the bottom) when the load is changed suddenly from about 50Ω to 100Ω. From this, it can be seen that the control voltage can respond immediately to keep the output voltage constant when load changes occur. The amount of power transferred varies between 11.52W ~ 5.76W with the load resistance changing between 50Ω and 100Ω and the output voltage kept consistent at 24V. In addition to changes in the load, the output voltage can also be kept stabilized between 23.5 V and 24.5 V with the coupling coefficient k between L_p and L_s changing between 0.57 and 0.66 in the experiment. The

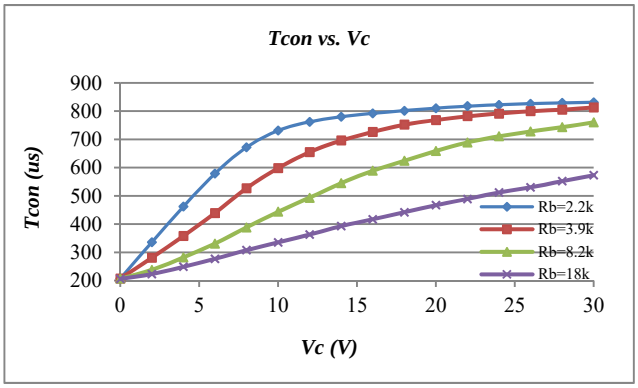

Fig. 14. The experimental relationships between T_{con} and V_c under different values of R_b.

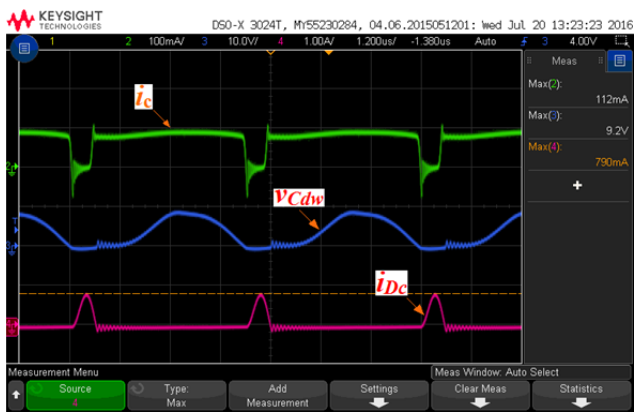

Fig.15. The experimental waveforms of i_c, v_{Cdw} and i_{Dc}.

power transfer efficiency changes between 86% and 75% according to the value of the control voltage V_c. The higher V_c is, the lower the efficiency because a higher V_c leads to a larger i_c and i_{Dc}, which result in a larger power dissipation by the transistor and diode. The power transfer efficiency is calculated as a ratio of the output power (V_{out}^2/R_{load}) to the input power (V_{Lp}*I_{Lp}), where V_{Lp} and I_{Lp} represent the effective value of the voltage and current of the primary coil L_p, respectively.

Fig. 14 shows the experimental relationship between T_{con} and V_c under different values of the base resistor R_b, which agrees relatively well with the simulation results shown in Fig. 7 in terms of the variation trend of T_{con} with V_c. However, it can be seen that the variation scopes of T_{con} with V_c are smaller in the experimental results shown in Fig. 14 (roughly between 200ns~830ns) than those of the simulation results shown in Fig. 7 (roughly between 0ns~1090ns). This is probably caused by differences between the parameters of the components in the simulation and in the practical experiments. In particular, the power dissipations of the components in the practical experiments may be larger than those in the simulations.

Fig. 15 shows steady state experimental waveforms of the collector current i_c, the voltage across the diode v_{Cdw} and the current of the diode i_{Dc} when the control voltage V_c is 5V and

the base resistor is 18k, which agrees relatively well with the simulation results shown in Fig. 5 in terms of the shape of the waveforms and the variation scope. Similarly, differences between the component parameters of the simulation and the practical circuit experimentation can cause errors between the simulation and practical experimentation results.

VI. CONCLUSIONS

This paper proposed a simple method to stabilize the output voltage of the secondary side of an IPT system by tuning/detuning through a DC Voltage-controlled Variable Capacitor (*DVVC*) combined with a PI controller. The equivalent capacitance of the *DVVC* is controlled by a DC voltage which influences the conduction period of a diode in the *DVVC*. Since no active switches are used in the *DVVC*, there are no active switch driving problems such as the need for a separate voltage source or gate drivers. This makes the *DVVC* especially advantageous when used at the secondary side of an IPT system. In the experiment, a 24V output voltage is used directly as the source of the PI controller, which generates the DC control voltage for the *DVVC* to make the output voltage stabilized at 24V, with the load and the coupling coefficient changing between 50Ω and 100Ω, and between 0.57 and 0.66, respectively. Experiments were carried out with Qi standard coils at 240 kHz to demonstrate the practical use of the proposed method. However, since the equivalent capacitance can be controlled smoothly by a DC voltage with a minimal EMI, the *DVVC* has the potential to be used at much higher frequencies than traditional switch mode capacitors.

REFERENCES

[1] A. P. Hu, "Selected resonant converters for IPT power supplies," Ph.D thesis, Electrical and Electonic Enginnering, The University of Auckland, 2001.

[2] D. Ahn and S. Hong, "Wireless power transmission with self-regulated output voltage for biomedical implant," *IEEE Trans. Ind. Electron.*, Vol. 61, No. 5, pp. 2225-2235, May 2014.

[3] Q. Chen, S. C. Wong, C. K. Tse, and X. Ruan, "Analysis, design, and control of a transcutaneous power regulator for artificial hearts," *IEEE Trans. Biomed. Circuits Syst.*, Vol. 3, No. 1, pp. 23-31, Feb. 2009.

[4] P. Si, A. P. Hu, S. Malpas, and D. Budgett, "A frequency control method for regulating wireless power to implantable devices," *IEEE Trans. Biomed. Circuits Syst.*, Vol. 2, No. 1, pp. 22-29, Mar. 2008.

[5] T. Mohamadi, "Working frequency in wireless power transfer for implantable biomedical sensors," in *International Conference on Electrical Engineering and Informatics (ICEEI)*, pp. 1-5, Jul. 2011.

[6] A. J. Moradewicz and M. P. Kazmierkowski, "Contactless energy transfer system with FPGA-controlled resonant converter," *IEEE Trans. Ind. Electron.*, Vol. 57, No. 9, pp. 3181-3190, Sep. 2010.

[7] M. W. Baker and R. Sarpeshkar, "Feedback analysis and design of RF power links for low-power bionic systems," *IEEE Trans. Biomed. Circuits Syst.*, Vol. 1, No. 1, pp. 28-38, Mar. 2007.

[8] J. L. Villa, J. Sallan, J. F. S. Osorio, and A. Llombart, "High-misalignment tolerant compensation topology for ICPT systems," *IEEE Trans. Ind. Electron.*, Vol. 59, No. 2, pp. 945-951, Feb. 2012.

[9] C. M. Zierhofer and E. S. Hochmair, "The class-E concept for efficient wide-band coupling-insensitive transdermal power and data transfer," in *14th Annual International Conference of the IEEE Engineering in Medicine and Biology Society*, pp. 382-383. Oct./Nov. 1992.

[10] G. Wang, W. Liu, M. Sivaprakasam, and G. A. Kendir, "Design and analysis of an adaptive transcutaneous power telemetry for biomedical implants," *IEEE Trans. Circuits Syst. I, Reg. Papers*, Vol. 52, No. 10, pp. 2109-2117, Oct. 2005.

[11] J. T. Boys, G. A. Covic, and Y. Xu, "DC analysis technique for inductive power transfer pick-ups," *IEEE Power Electronics Letters*, Vol. 99, No. 2, pp. 51-53, Jun. 2003.

[12] A. W. Green and J. T. Boys, "10 kHz inductively coupled power transfer-concept and control," in *Fifth International Conference on Power Electronics and Variable-Speed Drives*, pp. 694-699, Oct. 1994.

[13] J. T. Boys, G. A. Covic, and A. W. Green, "Stability and control of inductively coupled power transfer systems," *IEE Proceedings - Electric Power Applications*, Vol. 147, No. 1, pp. 37-43, Jan. 2000.

[14] A. Kumar and A. P. Hu, "Linearly tuned wireless power pick-up," in *IEEE International Conference on Sustainable Energy Technologies (ICSET)*, pp. 1-6, Dec. 2010.

[15] Y. Hiraga, J. Hirai, Y. Kaku, Y. Nitta, A. Kawamura, and K. Ishioka, "Decentralized control of machines with the use of inductive transmission of power and signal," in *Conference Record of the 1994 IEEE Industry Applications Society Annual Meeting*, pp. 875-881, Oct. 1994.

[16] A. Kumar, "Low power linearly tuned embeddable battery charging pick-up," Electrical and Electronic Engineering, University of Auckland, 2010.

[17] C.-Y. Huang, J. T. Boys, G. A. Covic, and M. Budhia, "Practical considerations for designing IPT system for EV battery charging," in *IEEE Vehicle Power and Propulsion Conference (VPPC)*, pp. 402-407, Sep. 2009.

[18] J. T. Boys and A. W. Green, "Inductively coupled power transmission:-concept, design and application," Transactions of the Institution of Professional Engineers New Zealand: Electrical / Mechanical / Chemical Engineering Section, Vol. 22, No. 1, p. 254, Nov. 1995.

[19] J. G. Ziegler and N. B. Nichols, "Optimum settings for automatic controllers," *Journal of Dynamic Systemns, Measurement, and Control*, Vol. 115, No. 2B, pp. 220-222, Jun. 1993.

[20] P. M. Meshram and R. G. Kanojiya, "Tuning of PID controller using Ziegler-Nichols method for speed control of DC motor," in *International Conference on Advances in Engineering, Science and Management (ICAESM)*, pp. 117-122, Mar. 2012.

[21] J. G. Ziegler and N. B. Nichols, "Optimum settings for automatic controllers," *Journal of Dynamic Systemns, Measurement, and Control*, Vol. 115, No. 2B, pp. 220-222, Jun. 1993.

[22] G. Mallesham, S. Mishra, and A. N. Jha, "Ziegler-Nichols based controller parameters tuning for load frequency control in a microgrid," in *International Conference on Energy, Automation, and Signal (ICEAS)*, pp. 1-8, Dec. 2011.

Jianlong Tian received his B.S. degree in Mechanical and Electric Engineering from the Agricultural University of Hebei, Baoding, China, in 1989; and his M.S. degree in Detection Technology and Automatic Equipment from the Beijing University of Chemical Technology, Beijing, China, in 2003. He has been working towards his Ph.D. degree at the University of Auckland, Auckland, New Zealand, since 2012. For more than eight years he worked as an Electronic Engineer for a couple of companies in Beijing, China. His current research interest include the high frequency and resonant operation of IPT systems, voltage controlled variable capacitors and soft-switching DC-AC power converters.

Aiguo Patrick Hu received his B.S. and M.S. degrees from Xian Jiaotong University, Xian, China, in 1985 and 1988, respectively; and his Ph.D. degree from the University of Auckland, Auckland, New Zealand, in 2001. He served as a Lecturer and as a Director of the China Italy Cooperative Technical Training Center in Xian, China, and as the General Manager of a technical development company. He stayed for a semester at the National University of Singapore (NUS), Singapore, as an Exchange Postdoctoral Research Fellow with funding from the Asian2000 Foundation. Patrick is a leading researcher in the field of wireless power technologies. He holds 15 patents in wireless/contactless power transfer and microcomputer control technologies, has published papers in more than 200 peer reviewed journal and conference proceedings and has over 2600 citations. He authored the first monograph on wireless inductive power transfer technology, and contributed 4 book chapters on inductive power transfer modeling/control as well as electrical machines. Patrick is currently with the Department of Electrical and Electronic Engineering, University of Auckland, Auckland, New Zealand. He is also the Head of Research of PowerbyProxi Ltd, as well as a Guest Professor of Chongqing University, Chongqing, China, and Taiyuan University of Technology, Taiyuan, China. He is a Senior Member of IEEE, a former Chairman of IEEE NZ Power Systems/Power Electronics Chapter, and the current Chairman of the NZ North Section. He served as Secretary/Treasurer of the NZ Chinese Scientists Association, and is now the Vice President. His current research interests include wireless/contactless power transfer systems, and the application of power electronics in renewable energy systems.

Sing Kiong Nguang received his B.S. (with first class honors) and Ph.D. degrees from the Department of Electrical and Computer Engineering of the University of Newcastle, Callaghan, Australia, in 1992 and 1995, respectively. He is presently working in the Department of Electrical and Computer Engineering, University of Auckland, Auckland, New Zealand. He has published over 300 papers in refereed journals and conference proceedings on the subjects of nonlinear control design, nonlinear control systems, nonlinear time-delay systems, nonlinear sampled-data systems, biomedical systems modeling, fuzzy modeling and control, biological systems modeling and control, and food and bioproduct processing. He has served on the editorial boards of a number of international journals. He is the Chief-Editor of the International Journal of Sensors, Wireless Communications and Control.